Journal of Machine Construction and Maintenance
QUARTERLY ISSN 1232-9312 1/2018(108)
p. 33–44

Zbigniew SIEMIĄTKOWSKI, Mirosław RUCKI
Kazimierz Pulaski University of Technology and Humanities in Radom, Poland
Faculty of Mechanical Engineering
z.siemiatkowski@uthrad.pl; m.rucki@uthrad.pl

Sergiy LAVRYNENKO
National Technical University "Kharkov Polytechnic Institute," Ukraine
lavr@kpi.kharkov.ua

INVESTIGATIONS ON THE MODELED SHRINK-FITTED JOINTS OF ASSEMBLED CRANKSHAFTS

Key words: mechanical engineering, shrink fittings, assembled crankshafts, large size engine.

Abstract: The paper describes the results of investigations on shrink-fitted joints. Models of the marine engine cranks and pivots were made in the scale of 1:5 considering real conditions of the large-sized crankshafts fabrication. The results of ultrasonic measurements of stresses were compared to the temperature distribution during the cooling process of the assembled couplings. The conclusion was that the unsteady stress distribution might be caused by the unsteady cooling process. The proposed model of the cooling process provided an explanation on how the stresses and deformations appear. As a consequence, more tight joints may not reveal a better ability to bear a torque load.

Badania modeli połączeń skurczowych składanych wałów korbowych

Słowa kluczowe: budowa maszyn, połączenia skurczowe, składane wały korbowe, silniki wielkogabarytowe.

Streszczenie: Przedstawiono wyniki badań nad połączeniami skurczowymi. Pomniejszone modele korb i czopów w skali 1:5 zostały wykonane z zachowaniem rzeczywistych warunków technologicznych dla okrętowych wałów korbowych. Wyniki pomiarów naprężeń metodą ultradźwiękową zostały porównane do rozkładów temperatur w czasie chłodzenia złożonych połączeń. Wykazano, że nierównomierny rozkład naprężeń może być wynikiem nierównomiernego przebiegu chłodzenia. Zaproponowano model procesu chłodzenia wyjaśniający sposób powstawania naprężeń i odkształceń w połączeniu skurczowym, które skutkują tym, że zwiększenie wcisku nie przekłada się na zwiększenie przenoszonego momentu skręcającego.

Introduction

There are three common technologies for the marine crankshaft fabrication. Unlike the fully forged crankshafts, production of the assembled and semi-built crankshafts that may be considered as the most common for large marine main engines involves the shrink fitting method [4]. For example, the crankshaft 6S35MC type is of 4,700 mm long, its crank radius is 700 mm, and the weight is 11,730 kg, and it is assembled in the vertical position. All of its elements, e.g., crankpin journal, main journal, and crankwebs, are prepared separately and joined together in an appropriate angle position with a shrink-fitting technology. Figure 1 presents the elements of such a crankshaft, and Fig. 2 shows how it looks after assembling.

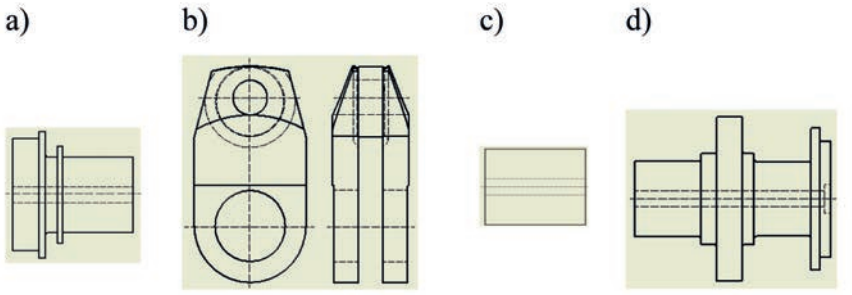

Fig. 1. Elements of the assembled crankshaft: a) supporting journal, b) crank, c) main journal, d) journal with flange [16]

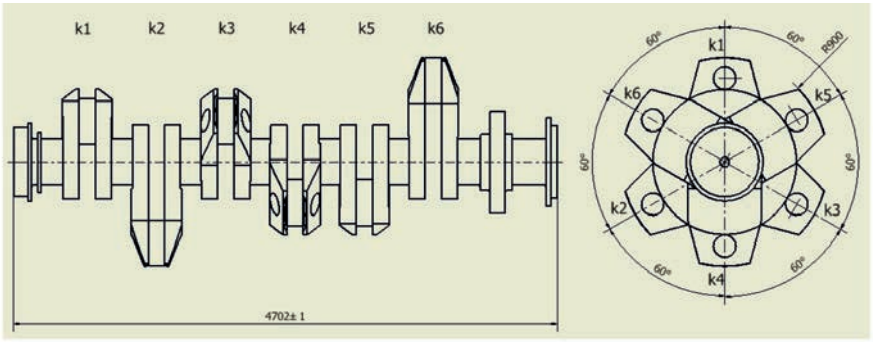

Fig. 2. Scheme of the assembled crankshaft

The crankshaft is a very responsible element of the marine engine, its failure, especially during the operation in the storm, may lead to a threat towards the lives of shipboard personnel and passengers. Moreover, the industrial design requires knowledge based on the investigation in the area of new materials and methods [10,12] and knowledge concerning surface morphology [7]. Because of safety reasons, the joints must be able to bear the increased load. To calculate the loading causing the shaft-hub detachment, Radi et al. [13] proposed an analytical model based upon the Lamé equation and the beam theory. In their solution, the shaft-hub contact was modelled in terms of two elastic Timoshenko beams connected by a distributed elastic spring. Its stiffness was evaluated analytically. It is known that fractures in crankshafts can occur by bending fatigue, by torsional fatigue, or a combination of both [5]. Moreover, in the assembled crankshafts, the hub must be axially positioned on the shaft and resist the moments and forces generated by misalignments [9]. However, it is known that the residual stresses and their distribution in mechanical components may cause them to fail at a load level significantly lower than expected [1]. Siemiatkowski [16] demonstrated experimentally that the relative interference above 2.2‰ did not improve the bonding strength of the shrink-fitted crank-pivot joint, and Burenin et al. [2] proved theoretically that plastic deformation in the shrink-fitted coupling under temperature stress significantly reduced its tightness. The effect of the shrink fitting ratios was investigated by Lee et al. [8], and Kim et al. [6] proposed a technique based on the 3D Finite Elements method for the shrink-fitting procedure optimization. Strozzi et al. [17] reported the results of a study on elastic stress concentration. Zhang et al. [20] studied the initiation characteristics of fretting fatigue cracks in the shrink-fitted shafts to analyse the wear mechanism.

1. Internal stress measurement in the models

There are many methods of the the analysis of shrink fit couplings in different applications [19], but, in case of such a large-sized elements, empirical investigation and measurement is extremely difficult and expensive. In particular, fabrication of the assembled crankshaft just for the residual stress measurement with the layer removal technique [3] would be financially too expensive.

Therefore, 1:5 scale models were made in order to make laboratory measurements possible [16]. The shrink fitted couplings were fabricated keeping technology as close to the technical conditions of large-sized crankshafts production as possible.

Surface topography has a crucial effect on the precision of the obtained parts [11]. Thus, roughness and form deviations of the models were measured in order to ensure the appropriate relative tightness of the couplings in the range between 2.0 and 2.5‰. The

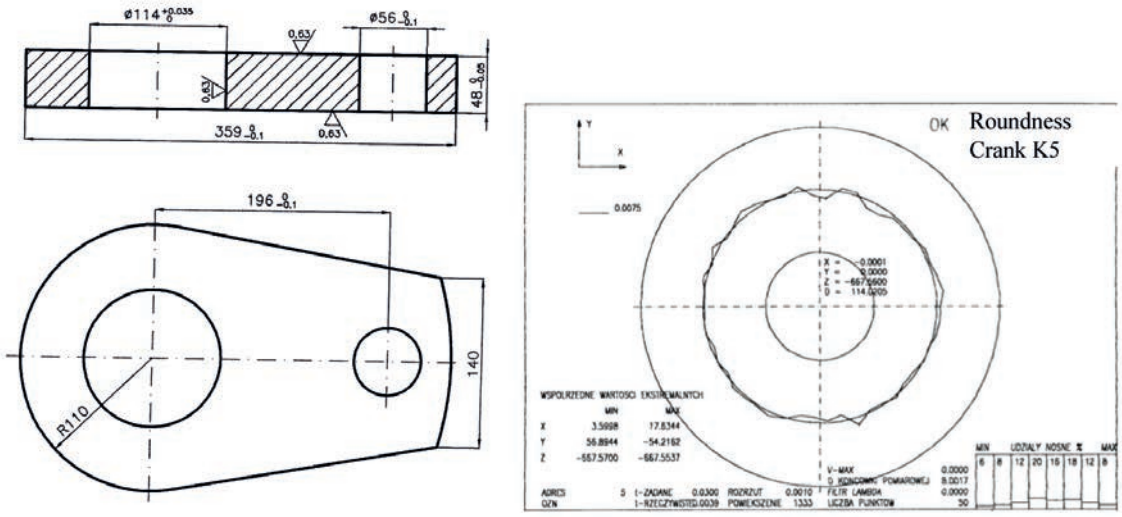

Fig. 3. An example of the investigated model of the crank (left) and the out-of-roundness of its orifice (right) [11]

roughness of the surfaces was kept between Ra = 0.32 and 0.40 μm. Examples of the examined models of the crank and the roundness measurements are shown in Fig. 3. The surfaces designed to be in contact were dried and degreased before the operation, but no substances increasing friction were applied. To complete shrink-fitted joints, each crank was heated in the area around its orifice up to the temperature of 350°C, while pivot was left at room temperature. After the pivot was inserted into the crank, the coupling was left to cool in ambient conditions.

The shrink-fitted elements generate internal stresses, which were measured using an ultrasonic measurement device (Debro) in the laboratory of the Institute of Fundamental Technological Research (Polish Academy of Sciences). For each couple, crank-pivot and ring-pivot, measurements were made before they were joined together and afterwards. Examples of measurement results for radial stresses in the assembled models are shown in Fig. 4.

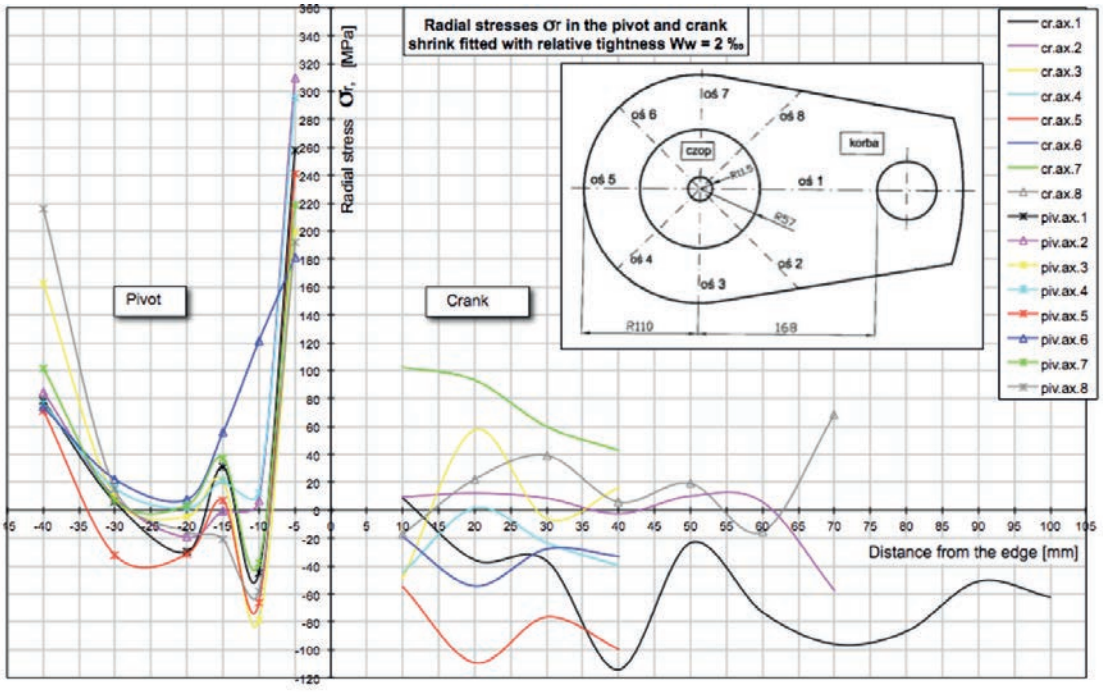

Fig. 4. An example of the measured radial stress distribution in the shrink-fitted crank and pivot along the axes [16]

The stress measurement results should be treated as the stresses averaged along the material thickness. In the case when they were performed close to the border between the details, they indicated the average along the joint. Both digital simulation and the hole-drilling strain-gage method confirmed the unsteady stress distribution [15]. The extension of the concentrated stress over the yield point is the factor most probably responsible for the reduced tightness of the shrink fit.

2. Calculations of the shrink fitted joints

The interferences between the pivot and crank were calculated with two methods: analytically as a thick-wall pipe with constant inner pressure, and using Finite Elements Method (FEM) as a pressure steadily applied to the inner surface of the crank bore. The results were obtained in form of stress distribution graphs and deformation diagrams.

The Lamé equations for the pressure p could be written for the known interference w as follows:

$$p = \frac{E \cdot w}{r_{zc}} \cdot \frac{(r_{zc}^2 - r_{wc}^2) \cdot (R_{zk}^2 - r_{zc}^2)}{2 \cdot r_{zc}^2 \cdot (R_{zk}^2 - r_{wc}^2)} \tag{1}$$

where

w – radial interference between the crank bore and pivot,

r_{wc}, r_{zc} – inner and outer radius of the shrink-fitted orifice and pivot, respectively,

R_{wk}, R_{zk} – inner radius of the crank bore and outer radius of its cylindrical part, respectively,

E – Young's modulus.

Assuming that the interference w is the difference between the displacements of the pivot u_{cz} and the one of crank u_k, it could be written:

$$w = u_{cz} - u_k \tag{2}$$

Thus, it can be written:

$$u_{cz} = -\frac{r_{zc} \cdot p}{E} \left(\frac{r_{wc}^2 + r_{zc}^2}{r_{zc}^2 - r_{wc}^2} - v \right) \tag{3}$$

$$u_k = \frac{R_{wk} \cdot p}{E} \left(\frac{R_{wk}^2 + R_{zk}^2}{R_{zk}^2 - R_{wk}^2} - v \right) \tag{4}$$

where ν – Poisson's constant.

The stresses, both radial σ_r and tangential σ_t in the pivot and crank, are calculated from the following equations:

a) For the pivot:

$$\sigma_{r(cz)} = \frac{r_{zc}^2 \cdot p}{r_{zc}^2 - r_{wc}^2} \left(\frac{r_{wc}^2}{r^2} - 1 \right) \tag{5}$$

$$\sigma_{t(cz)} = -\frac{r_{zc}^2 \cdot p}{r_{zc}^2 - r_{wc}^2} \left(\frac{r_{wc}^2}{r^2} + 1 \right) \tag{6}$$

where r is the current radius of the pivot from the range $\langle r_{wc}; r_{zc} \rangle$.

b) For the crank:

$$\sigma_{r(k)} = \frac{R_{wk}^2 \cdot p}{R_{zk}^2 - R_{wk}^2} \left(1 - \frac{R_{zk}^2}{R^2} \right) \tag{7}$$

$$\sigma_{t(k)} = \frac{R_{wk}^2 \cdot p}{R_{zk}^2 - R_{wk}^2} \left(1 + \frac{R_{zk}^2}{R^2} \right) \tag{8}$$

where R is the current radius of the crank from the range $\langle R_{wk}; R_{zk} \rangle$, which enables to calculate the stress distribution.

Based on the von Mises–Huber's hypothesis, the reduced stresses for the pivot $\sigma_{red(cz)}$ and the ones for the crank $\sigma_{red(k)}$ can be calculated from the Equations (9) and (10), respectively:

$$\sigma_{red(cz)} = \sqrt{\sigma_{r(cz)}^2 + \sigma_{t(cz)}^2 - \sigma_{r(cz)} \cdot \sigma_{t(cz)}} \tag{9}$$

$$\sigma_{red(k)} = \sqrt{\sigma_{r(k)}^2 + \sigma_{t(k)}^2 - \sigma_{r(k)} \cdot \sigma_{t(k)}} \tag{10}$$

In the above equations, the following values were input: $E = 2.1 \times 10^5$ MPa, $r_{wc} = 11.5$ mm, $r_{zc} = R_{wk} = 57.0$ mm, $R_{zk} = 110.0$ mm, $\nu = 0.3$, and the interference $w = 0.1275$ mm.

The obtained results are as follows:

a) For the maximal radial interference $w = 0.1275$ mm, the relative tightness was $W_r = 2.24‰$, the pressure in the joint $p = 167$ MPa, the crank radius increase $u_k = 0.092$ mm, and the pivot radius decrease $u_{cz} = -0.035$ mm.

b) For the minimal radial interference $w = 0.117$ mm, the relative tightness was $W_r = 2.05‰$, the pressure in the joint $p = 153$ MPa, the crank radius increase $u_k = 0.084$ mm, and the pivot radius decrease $u_{cz} = -0.033$ mm.

The graph of calculated pressure in the shrink-fitted pivot and crank is presented in Fig. 5, and the stress distribution is presented in Fig. 6.

It can be also calculated that the maximal bearable torque for the shrink-fitted coupling is as follows:

$$Ms_{\max} = 2 \cdot \mu \cdot \pi \cdot R_p^2 \cdot L \cdot p \tag{11}$$

where

μ – friction coefficient,

R_p – nominal radius of the shrink-fitting,

L – axial length of the interference, equal to the crank thickness.

In the experimental model, the theoretical pressure was p = 167 MPa, nominal radius $R_p = R_{wk} = r_{zc}$ = 57 mm, contact length L = 48 mm, and friction coefficient was μ = 0.2. Thus, the maximal torque was calculated as Ms_{max} = 32.7 kNm.

Figure 7 presents the examples of the stresses compared to the deformations calculated with the Finite Elements Method (FEM), and Fig. 8 shows the examples of the components of stresses in different directions.

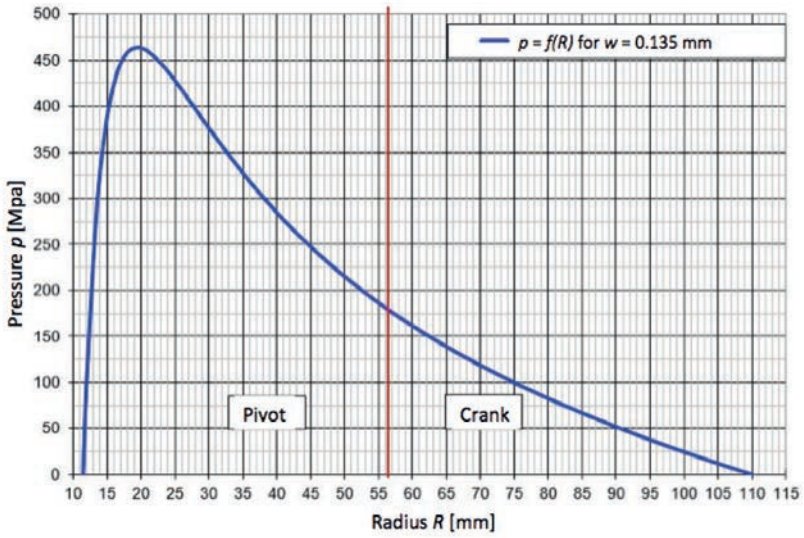

Fig. 5. Theoretical (Lamé) pressure distribution in the pivot and crank for the interference w = 0.1275 mm

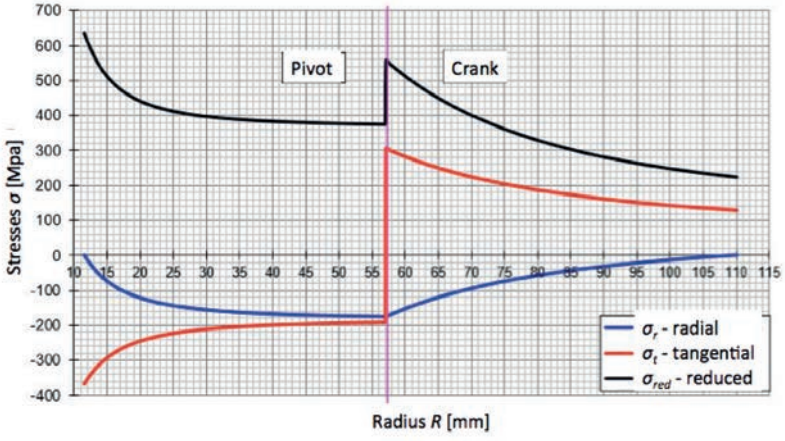

Fig. 6. Theoretical (Lamé) stresses in the shrink-fitted pivot and crank for the radius R = 57 mm and interference w = 0.1275 mm

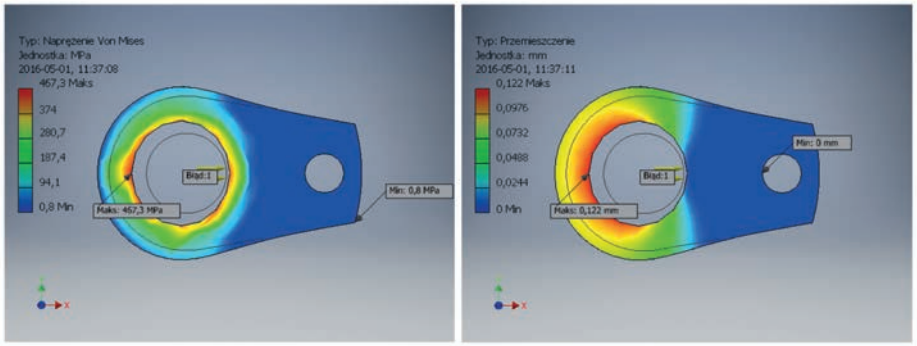

Fig. 7. Reduced stresses $\sigma_{red(k)}$ (left) and deformations (right) in the crank

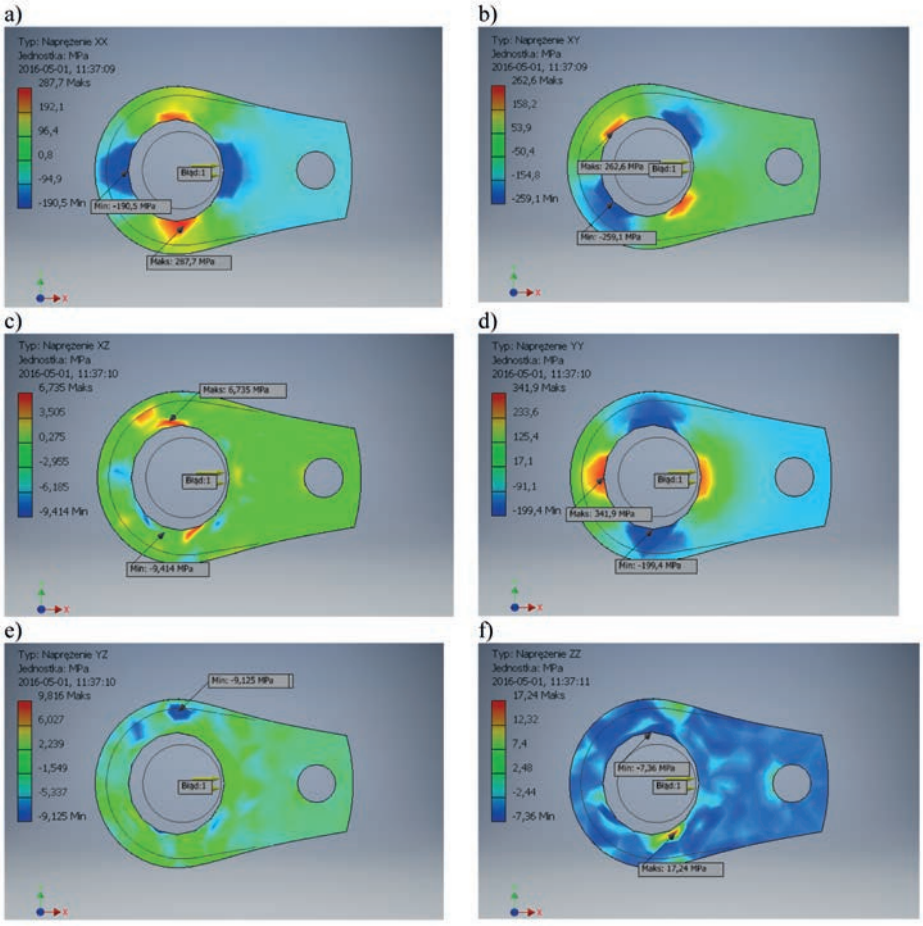

Fig. 8. Components of the stress tensor in the crank in different directions: a) XX, b) XY, c) XZ, d) YY, e) YZ, f) ZZ

From Figures 7 and 8, it can be seen that the crank geometry generates a specific kind of stress during the shrinkage and the rise of respective pressure on the crank bore. As a result of unsteady and irregular stresses, deformation takes place, so the axis of the crank bore moves along the *X*-axis. The maximal von Mises stresses can be seen in the front side of the cylindrical part of the crank. In Fig. 7 (left), the place where the maximal reduced stress σ_{redmax} = 467.3 MPa appears is marked. Similarly, the maximal displacement 0.122 mm is seen in the front side, where the maximal stress appeared (Fig. 7 right), while the minimal one takes place on the back side. The abovementioned phenomenon is caused by the varying stiffness of the crank in the radial direction from the crank bore.

3. The experimental rig for the shrink-fitted joint temperature measurement

Apart from the stress measurements, the local temperature was measured in the area of joint between cranks and pivots or rings and pivots, respectively. In order to perform the measurement and distribution analysis of the temperature during the cooling process of the shrink-fitted joint, a dedicated experimental rig was made. The equipment made it possible to simulate the full assembling cycle of the pivot with crank, i.e. heating, insert of the pivot into bore, and the cooling of the coupling. The experimental setup is shown in Fig. 9.

During the measurement, the model crank (1) is placed on the supports (2) of height projected in the scale 1:5 related to the real dimensions of the assembled marine diesel engine crankshaft. From the bottom side, the burner is placed to heat the examined element up to 350ºC.

In the special measurement ring (5), eight independent thermocouples PTT-K (NiCr – NiAl) were placed (6). They were distributed at 45º increments (Fig. 4 above), and their measurement diameters were 10 mm and thickness 1 mm. The measurement ring was placed in a way that ensured a small pressing force on the crank surface around the bore. The special pads and silicon lubricator provided appropriate heat transfer and electric isolation between thermocouples.

The thermocouples were connected with the measurement card (DAC-pad 71B) produced by

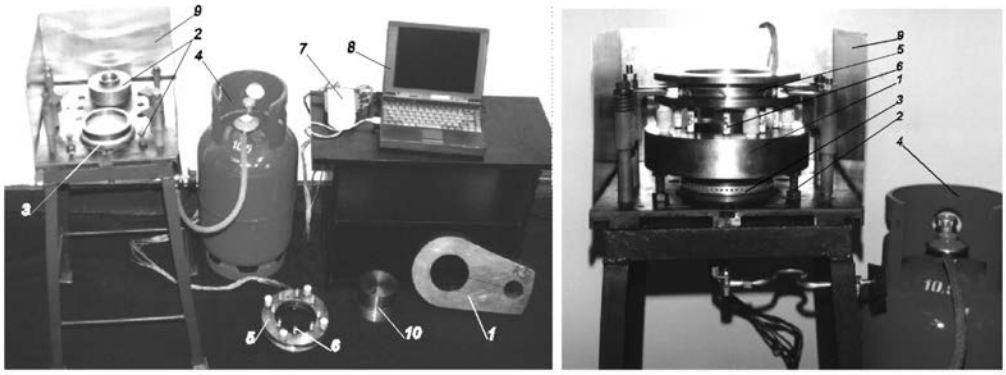

Fig. 9. The experimental rig for the temperature measurement (details explained in the text)

"Advantech" (7). The card was installed in a computer (Aristo FT-6000E) equipped with a Pentium 120 processor (8). The measurement card made it possible to perform temperature compensation. The thermocouples were adjusted at the temperature of 0ºC.

The metal plate cover (9) eliminated the noises that may affect the measurement results, especially those caused by the air swirling around the measurement area. The signal sampling was made with a frequency 30 kHz. The measurement inaccuracy was estimated at the level of 2% on the basis of the comparative test measurement.

The locations of the temperature measurements and an example of the graphs obtained for each sensor during the cooling are shown in Fig. 10.

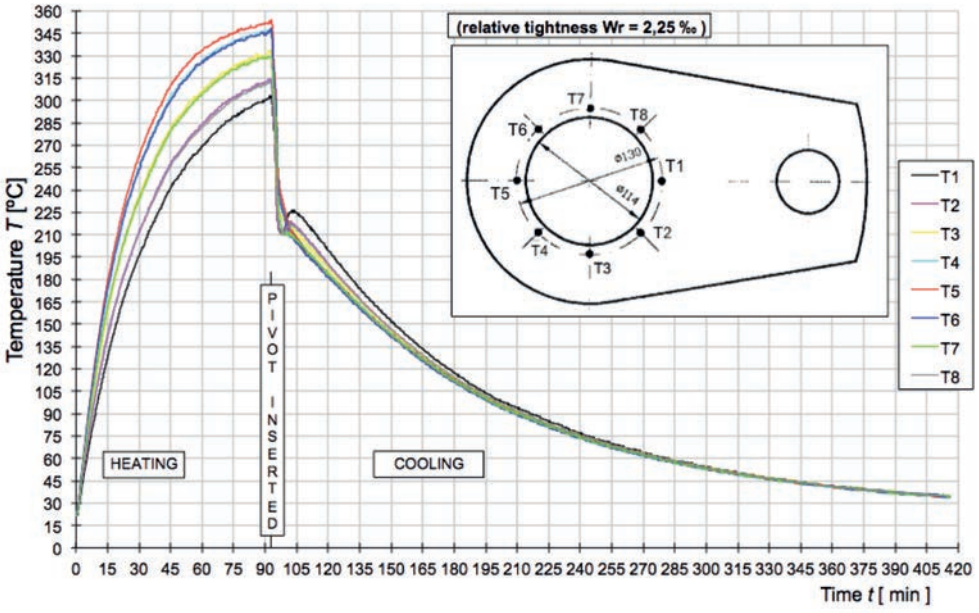

Fig. 10. The temperature registered by the sensors T1-T8 during the cooling in the air

4. Measurement results and discussion

The temperature is closely related to the dimensional changes of the heated crank and its bore diameter. Theoretical calculation was made for the ideal assumption of proportional linear diameter change ΔD at the mean temperature obtained from the opposite thermocouples, e.g., T1 and T5 or T3 and T7. The following formula was applied:

$$\Delta R_{wk} = R_{wk}\, \alpha\, \Delta T \tag{12}$$

where

R_{wk} – crank bore radius,

α – linear thermal expansion coefficient (for steel S34MnV $\alpha = 14 \times 10^{-6}$ [1/ºC]),

ΔT – absolute increase of the temperature on the crank surface.

The differences between the theoretical and measured values of ΔD did not exceed 0.02 mm. The results for the same crank (relative tightness W_r = 2.25‰) are presented in the Table 1. The problem, however, appears because the axis of the crank bore is moving during the heating process. For example, for the same crank, the radiuses related to the thermocouples T1 and T5 increase for the values ΔR_c (T1) = 0.226 mm and ΔR_c (T5) = 0.265 mm, respectively. The illustrations of the thermal deformation resulting in the axis movement are shown in Fig. 11.

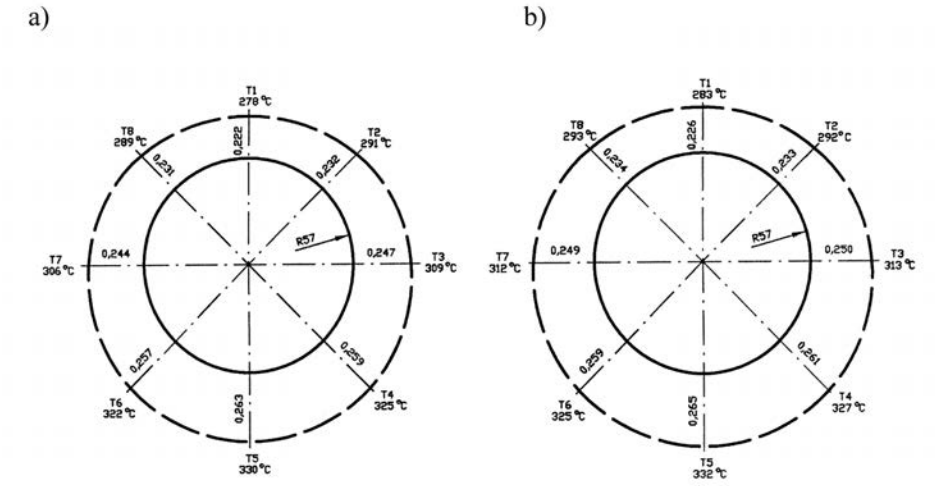

Fig. 11. Thermal deformation of the crank bore immediately before insertion of pivot: a) for the relative tightness W_r = 2.25‰, b) for the relative tightness W_r = 2.00‰

Table 1. Increase of the bore diameter during the crank heating process

Heating time t [min]	Mean absolute increase of the temperature around the bore in the crank				Measured increase of the diameter between two corresponding thermocouples				Calculated increase of the diameter between two corresponding thermocouples			
	(T1+T5)/2 [ºC]	(T2+T6)/2 [ºC]	(T3+T7)/2 [ºC]	(T4+T8)/2 [ºC]	DD1 [mm]	DD2 [mm]	DD3 [mm]	DD4 [mm]	DD1 [mm]	DD2 [mm]	DD3 [mm]	DD4 [mm]
0	0	0	0	0	0	0	0	0	0	0	0	0
10	93	98	100	97	0.14	0.15	0.15	0.15	0.15	0.16	0.16	0.15
20	162	166	168	165	0.25	0.25	0.25	0.25	0.26	0.26	0.27	0.26
30	207	210	213	211	0.33	0.32	0.32	0.32	0.33	0.34	0.34	0.34
40	240	243	245	243	0.39	0.38	0.38	0.38	0.38	0.39	0.39	0.39
50	263	267	268	267	0.42	0.41	0.41	0.41	0.42	0.43	0.43	0.43
60	279	283	283	282	0.45	0.44	0.44	0.44	0.45	0.45	0.45	0.45
70	290	294	296	293	0.47	0.47	0.47	0.46	0.46	0.47	0.47	0.47
80	299	301	303	302	0.48	0.48	0.48	0.48	0.48	0.48	0.48	0.48
90	304	306	307	307	0.49	0.49	0.49	0.49	0.48	0.49	0.49	0.49

As reported in other papers, e.g., Sun et al. [18], there is a difference between the heating time of the pin side and round side around the bore. In the current study, the most interesting observation of the cooling process is the slight increase of the crank temperature near the bore after the initial fall to the value of ca. 210ºC. As it is seen in Fig. 10 above, such an increase is indicated by the thermocouples T1, T2, and T8 placed where there is much more material to be cooled than in case of the other thermocouples. No phenomenon of that kind takes place in the case of the ring-type detail, as shown in Fig. 12.

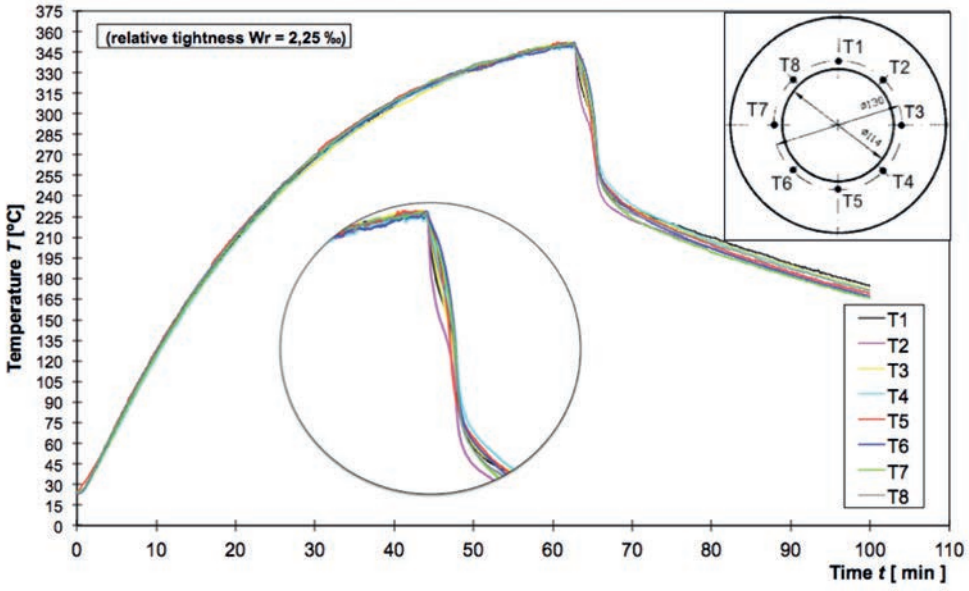

Fig. 12. Graph of the temperature during the shrink-fitting process for the ring and pivot of relative tightness W_r = 2.25‰

Moreover, Fig. 12 indicates another problem with unsteady cooling. After the pivot is inserted, the thermocouple T2 indicates evidently quicker cooling to ca. 300ºC than the other ones. At ca. 280ºC, the cooling speed becomes almost equal, but again, T5 reaches 235ºC more quickly than other thermocouples. This may be the evidence of non-axial insertion of the pivot, which resulted in increased heat transfer along the main contact line between the pivot and bore.

From Fig. 10, an additional explanation can be derived for the deformation mentioned above. At the time when the pivot is to be inserted into the crank bore, the difference between the temperature at the points T1 and T5 is ca. 55ºC. This fact results from the deformation of axis, even though the mean temperature for ΔD1 is almost the same as for other diameters (304ºC compared to 306 and 307). Sun at al. [18] reported that the displacement of centre of the bore may reach 0.5 mm, coaxially it may be distorted by 0.4–0.9 mm, and a rotation of 0.044° may occur.

The obtained measurement results led to conclusion that the inevitably unsteady cooling process is the main source of irregular shrinkage and subsequent unsteady distribution of the residual stresses that also result with the deformations of the assembled crankshaft. To understand it better, the cooling process may be divided to four stages, as follows:

– Immediately after the pivot is inserted to the hot crank bore, the heat transfer goes faster on the outer surfaces of crank than along the surface inside the bore. As a result, the upper and lower edges of the bore are shrinking faster and getting in contact with the cold pivot as shown in Fig. 13a.
– The contact circles around the pivot provide more intensive heat transfer than the rest of joint where air remains between the hot crank bore surface and the cold pivot surface. The pivot receives heat and expands, so its length and diameter increase, and simultaneously, it is squeezed by the shrinking crank bore. The contact circles grow into tight rings in the upper and lower parts of fitting (Fig 13b).
– The heat transfer and dynamic gradient of temperature cause deformations of both coupled elements. The axial extension of the pivot after the appearance of tight rings results in different contract forces between the pivot and crank bore. The most important and dominant force is the radial interference force p, but axial friction forces F_1 and F_2 directed against one another inevitably appear, as shown in Fig. 13c.
– The last stage starts when the pivot reaches its highest temperature and the coupling is cooled down together. The shrinking process is finished and interference fit is formed with its residual stress that provides the desired bonding strength. However, the resulting boundary surface is formed in the way presented ideally in Fig. 13d; however, in reality, it is more deformed and also has gaps as reported by other researchers [18].

These 4 stages of the cooling process provide the explanation on how the stresses are being generated in the large size assembled crankshaft and why their concentration leads to the reduced bonding strength. The deformations found after the reported destructive tests [16] stay in conformity with the above explanation.

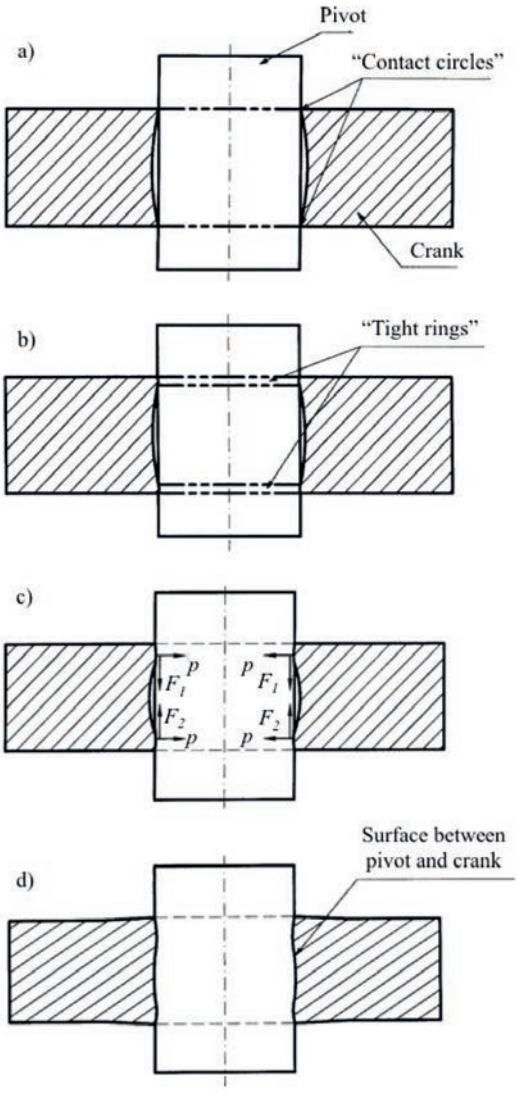

Fig. 13. Important stages of the cooling process: a) first "contact circles" between hot crank bore and cold pivot, b) appearance of the tight rings, c) growth of the shrinking force *p* and friction forces *F*, d) resulting boundary surface

Conclusions

The present study enabled us to indicate some important problems concerning the shrink-fitting technology applied in assembling large-size marine diesel engine crankshafts. First of all, temperature measurements provided a better understanding of the process. Secondly, residual stress calculations were performed according to the Lamé method and using the Finite Elements Method. Thirdly, deformations were analysed, and theoretical expectations were compared with experimental results. And finally, a model of the process was proposed based on the obtained results.

It was found that, in any analysis and project works, the shrink-fitting procedure should be divided into three stages: heating, insertion, and cooling. In the cooling process, unsteady temperature distribution is caused by the different thickness of the material around the bore. The registered temperature difference at the bore opposite sides reached 55ºC.

Next, the insertion of the pivot into the crank bore causes the rapid fall of the temperature, which may end with a slight temperature increase before the proper cooling process starts. No such increase of the temperature takes place in the ring-pivot shrink-fitting process. In some cases, when the pivot is inserted non-axially, the temperature may decrease more quickly along the main contact line.

The last phase of the procedure, the cooling, is responsible for the appropriate joint between the crank bore and the pivot squeezed in it. During the cooling process, the stresses cause the displacement of the crank

bore axis. The analysis of stages of the cooling process gave some explanation on why the resulting surface between shrink-fitted crank and pivot is not cylindrical and the residual stress distribution is unsteady.

The presented researches can be the basis for some practical recommendations, as follows:

– It is not advantageous to make the joint too tight, because the unsteadiness of process itself will generate larger deformations making the joint weaker.
– The deformation and stress distributions should be calculated taking into consideration unsteady heat transfer in different directions.
– Simplified calculations may result in much larger deformations than expected, including the axis displacement.

The abovementioned processes should be taken into consideration from the very beginning of the project stage, in order to keep the accuracy and reliability of the shrink-fittings in the assembled diesel marine crankshaft.

Acknowledgement

The article is the extended version of the paper that was originally presented at the conference M2D2017 (ref. number 6538), Albufeira/Portugal, 11–15 June 2017.

Funding sources

This research did not receive any specific grant from funding agencies in the public, commercial, or not-for-profit sectors.

References

1. Baldi, A., 2016. Using Optical Interferometry to Restart the Ring-Core Method. Experimental Mechanics 56, 1191–1202.
2. Burenin, A.A., Dats, E.P., Tkacheva, A.V., 2014. On the modeling of the shrink fit technology. Journal of Applied and Industrial Mathematics 8, 493. DOI 10.1134/S199047891404005X.
3. Carpenter, H.W., Reid, R.G., Paskaramoorthy, R., 2014. Extension of the layer removal technique for the measurement of residual stresses in layered anisotropic cylinders. International Journal of Mechanics and Materials in Design 10(3), 269–280. DOI 10.1007/s10999-014-9245-2
4. Fonte, M., Duarte, P., Anes, V., Freitas M., Reis, L., 2015. On the assessment of fatigue life of marine diesel engine crankshafts. Eng. Fail. Anal. 56, 51–57, DOI 10.1016/j.engfailanal.2015.04.014
5. Jadhav, A., Chalwa, V., Gaikwad, P., 2013. Fatigue Failure Analysis Of Marine Engine Crankshaft. International Journal of Engineering Research & Technology 2, 614–621.
6. Kim, H.Y., Kim, C., Bae, W.B., Han, S.M., 2007. Development of optimization technique of warm shrink fitting process for automotive transmission parts (3D FE analysis), Journal of Materials Processing Technology 187–188, 458–462. DOI 10.1016/j.jmatprotec.2006.11.107.
7. Krolczyk G.M., Maruda R.W., Nieslony P., Wieczorowski M., 2016. Surface morphology analysis of Duplex Stainless Steel (DSS) in Clean Production using the Power Spectral Density, Measurement, 94, 464–470. DOI 10.1016/j.measurement.2016.08.023.
8. Lee, H.C., Saroosh, M.A., Song, J.H., Im, Y.T., 2009. The effect of shrink fitting ratios on tool life in bolt forming processes, Journal of Materials Processing Technology 209, 3766–3775. DOI 10.1016/j.jmatprotec.2008.08.032.
9. Mancuso, J.R., 1999. Couplings and Joints: Design, Selection & Application. Marcel Dekker, Inc., New York – Basel.
10. Maruda R.W., Krolczyk G.M., Nieslony P., Wojciechowski S., Michalski M., Legutko S., 2016. The influence of the cooling conditions on the cutting tool wear and the chip formation mechanism, Journal of Manufacturing Processes, 24P1, 107––115. DOI 10.1016/j.jmapro.2016.08.006.
11. Nieslony P., Krolczyk, G.M., Wojciechowski, S., Chudy R., Zak K., Maruda R.W., 2018. Surface quality and topographic inspection of variable compliance part after precise turning, Applied Surface Science 434, 91–101. DOI 10.1016/j.apsusc.2017.10.158.
12. Nieslony P., Krolczyk G.M., Zak K., Maruda R.W., Legutko S., 2017. Comparative assessment of the mechanical and electromagnetic surfaces of explosively clad Ti-steel plates after drilling process, Precision Engineering, 47, 104 –110. DOI 10.1016/j.precisioneng.2016.07.011.
13. Radi, E., Lanzoni, L., Strozzi, A., Bertocchi, E., 2017. Shaft-hub press fit subjected to bending couples: Analytical evaluation of the shaft-hub detachment couple, Applied Mathematical Modelling 50, 135––160. DOI 10.1016/j.apm.2017.05.018.
14. Siemiatkowski, Z., 2017. Experimental evaluation of the shrink-fitted joints in the assembled crankshafts, Journal of Engineering Technology 6(2), 832–841.
15. Siemiątkowski, Z., Rucki, M., Kudlacek, J., 2018. Internal Stresses Analysis in the Shrink-Fitted Joints of the Assembled Crankshafts. In: Hamrol A., Ciszak, O., Legutko, S., Jurczyk, M. (Eds.), Advances in Manufacturing. Springer, Poznań, pp. 633–640. DOI 10.1007/978-3-319-68619-6_60.

16. Siemiatkowski, Z., Rucki M., Lavrynenko S., 2017. Investigations of the shrink-fitted joints in assembled crankshafts. In: Silva Gomes J.F., Meguid, S.A. (Eds.), Proceedings of the 7th International Conference on Mechanics and Materials in Design, Albufeira, Portugal, pp. 1155–1158.
17. Strozzi, A., Bertocchi, E., Baldini, A., Mantovani, S., 2016. Normalization of the stress concentrations at the rounded edges of an interference fit between a solid shaft subjected to bending and a hub. Mechanics Based Design of Structures and Machines 44(4), 405–425. DOI 10.1080/15397734.2015.1086274.
18. Sun, M.Y., Lu, S.P., Li, D.Z., Li, Y.Y., Lang, X.G., Wang, S.Q., 2010. Three-dimensional finite element method simulation and optimization of shrink fitting process for a large marine crankshaft. Materials and Design 31, 4155–4164. DOI 10.1016/j.matdes.2010.04.027.
19. Wang, X., Liu, B., Gao, K., Meng, Q., Sun, Y., 2016. Analysis of thermal deformation and influencing factors in shrink-fitting assembly of aluminum alloy drill pipe. Advances in Mechanical Engineering, 8(10), 1–15. DOI 10.1177/1687814016674099.
20. Zhang, Y., Lu, L., Gong, Y., Zhang, J., Zeng, D., 2017. Fretting wear-induced evolution of surface damage in press-fitted shaft, Wear 384-385, 131––141. DOI 10.1016/j.wear.2017.05.014.